iScience

CellPress
OPEN ACCESS

Article

Iridium(III) complexes with 1-phenylisoquinoline-4-carbonitrile units for efficient NIR organic light-emitting diodes

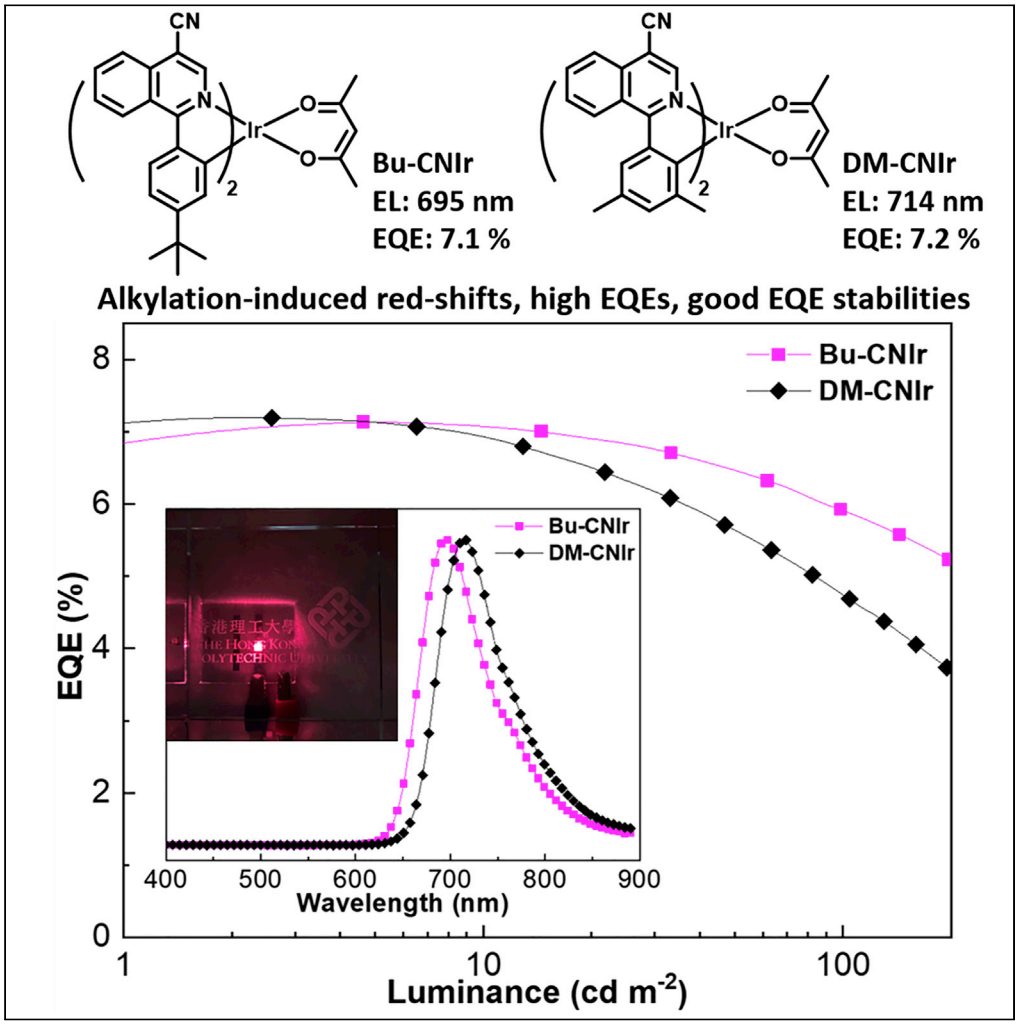

Hongyang Zhang, Yuqing Xu, Zhao Chen, Shuming Chen, Rong Liu, Wai-Yeung Wong

chenzhao2006@163.com (Z.C.)
chensm@sustech.edu.cn (S.C.)
rong.liu@polyu.edu.hk (R.L.)
wai-yeung.wong@polyu.edu.hk (W.-Y.W.)

Highlights

Efficient NIR-emitting Ir(III) phosphors are attained via three synthetic steps

Cyano and alkyl groups exert different effects on the properties of complexes

NIR OLEDs exhibit a maximum EQE of 7.2% with an emission peak at 714 nm

High current densities are recorded as peak EQEs are dropped to their half values

Zhang et al., iScience *24*, 102911
August 20, 2021 © 2021 The Author(s).
https://doi.org/10.1016/j.isci.2021.102911

iScience

CellPress
OPEN ACCESS

Article

Iridium(III) complexes with 1-phenylisoquinoline-4-carbonitrile units for efficient NIR organic light-emitting diodes

Hongyang Zhang,[1,2] Yuqing Xu,[3] Zhao Chen,[4,*] Shuming Chen,[5,*] Rong Liu,[1,*] and Wai-Yeung Wong[1,2,6,*]

SUMMARY

Achieving the high external quantum efficiency (EQE) of near-infrared (NIR) emission in iridium(III) complexes still remains a challenge owing to their unsteady excited states which easily decay to the ground states through the nonradiative pathways. Herein, three Ir(III) phosphors in which the cyclometalated ligand 1-phenylisoquinoline-4-carbonitrile (piq-CN) is functionalized with the cyano, *tert*-butyl, and dimethyl groups are developed (CN-CNIr, Bu-CNIr, and DM-CNIr, respectively). Three simple synthetic steps can afford this class of deep red to NIR Ir(III) emitters. The organic light-emitting diodes (OLEDs) based on Bu-CNIr and DM-CNIr attain the maximum EQEs of 7.1% and 7.2% with the emission peaks at 695 and 714 nm, respectively. This strategy using substituted piq-CN derivatives as the cyclometalated ligands can offer an effective approach to promote the radiative rate of NIR-emitting Ir(III) materials. An insight into how the electron-withdrawing and electron-donating substituents on ligands influence the optoelectronic properties of their Ir(III) complexes is also provided.

INTRODUCTION

Near-infrared (NIR) emitting materials have been demonstrated to give a full scope to photo immunotherapy (Li et al., 2020a, 2020b; Abdurahman et al., 2016), bioprobe/bioimaging (Maldiney et al., 2014; Wang et al., 2013, 2017), telecommunications (Bunzli and Eliseeva, 2010), information-secured displays (Baride et al., 2015; Kumar et al., 2016), organic light-emitting diodes (OLEDs) (Zampetti et al., 2019), and even solar energy conversion (Richards 2006; Der Ende et al., 2009). In general, the commonly used NIR emitting materials consist of inorganics (such as nanocrystals (Mao et al., 2014) and quantum dots (Pichaandi and Van Veggel, 2014)) and organic molecules (including organic fluorophores (Qian and Wang, 2010), transition-metal-based phosphors (Xiang et al., 2013), and so on). To achieve efficient organic NIR emitters, thermally activated delayed fluorescence (TADF) organics (Kim et al., 2018a) and organometallic phosphors based on Pt(II) (Ly et al., 2017), Os(II) (Liao et al., 2015), and Ir(III) complexes (Kim et al., 2018b) which can harness the energy of both 25% singlet and 75% triplet excited states are the most studied materials for getting high EQEs. Meanwhile, the luminescent radicals whose emissions originate from a spin doublet (Peng et al., 2015) are also considered to be one candidate material because the neutral radicals are capable of circumventing the efficiency limitations imposed by the triplet excitons. Under a designed structure of radical-based OLEDs, the selective injections of holes into the highest occupied molecular orbital (HOMO) and electron into the highest singly occupied molecular orbital (SOMO) could be achieved to form the emissive doublet excited state with near 100% internal quantum efficiency (IQE). However, if both electrons and holes occupy the SOMO level and recombine, doublet excited states for spin-allowed emission cannot be realized (Ai et al., 2018). On the other hand, the TADF emitters would go through a process in which triplet excitons are transferred into singlet ones via the efficient reverse intersystem crossing (RISC), providing the practicability of near-unity exciton utilization. Nevertheless, obvious EQE roll-offs are often observed at high current densities in TADF-emitter-based OLEDs (Xue et al., 2019; Zhang et al., 2019), and the intermolecular interactions of TADF organics are susceptible to their doping concentration in the emissive layer (EML), leading to the concentration-dependent peak emission wavelength of their OLED devices. For example, the nondoped OLED based on mDPBPZ-PXZ exhibits a deep red (DR)/NIR emission at 680 nm, while the corresponding doped (14 wt %) device shows a blue-shifted wavelength by over 50 nm to the red electroluminescence (EL) (Chen et al., 2019).

[1]Faculty of Applied Science and Textiles and Research Institute for Smart Energy, The Hong Kong Polytechnic University (PolyU), Hung Hom, Hong Kong, P. R. China

[2]PolyU Shenzhen Research Institute, Shenzhen 518057, P. R. China

[3]College of Physics and Optoelectronic Engineering, Ludong University, Yantai 264025, P. R. China

[4]School of Applied Physics and Materials, Wuyi University, Jiangmen 529020, P. R. China

[5]Department of Electrical and Electronic Engineering, Southern University of Science and Technology, Shenzhen 518000, P. R. China

[6]Lead contact

*Correspondence: chenzhao2006@163.com (Z.C.), chensm@sustech.edu.cn (S.C.), rong.liu@polyu.edu.hk (R.L.), wai-yeung.wong@polyu.edu.hk (W.-Y.W.)

https://doi.org/10.1016/j.isci.2021.102911

This is an open access article under the CC BY-NC-ND license (http://creativecommons.org/licenses/by-nc-nd/4.0/).

Transition-metal-based complexes have always been considered as one of the most promising light-emitting materials as the intersystem crossing (ISC) from the singlet excited state to triplet excited state can be facilitated and the spin-forbidden transition from the triplet excited state to ground state can be relaxed owing to the heavy atom effect, and hence, they are capable of achieving IQE of 100%. The square-planar Pt(II) complexes with strong Pt···Pt interactions can generate the strong intermolecular charge transfer transition including metal-metal-to-ligand charge transfer (^{3}MMLCT) in the trimers/oligomers which would lead to the remarkably red-shifted luminescence and are less susceptible to exciton-vibration coupling law (Wang et al., 2020; Chen et al., 2020a). As a result, their fabricated NIR OLEDs offered the peak EQE up to 24%, a record for the NIR OLEDs (Ly et al., 2017). Meanwhile, octahedral Os(II) complexes are proved to have relatively strong metal-to-ligand charge transfer (MLCT) contributions and high radiative rate constants so that the NIR OLEDs fabricated using them as the emitters also exhibit excellent EL performances. For example, the Os(II) phosphors using pyrazinyl azolate compounds as the cyclometalated ligands furnished the OLEDs a maximum EQE of 11.5% at the emission wavelength of 710 nm (Yuan et al., 2020). Therefore, a significant improvement on the EQEs of NIR OLED devices based on Pt(II) and Os(II) complexes has been attained in recent years. However, the diversity and/or variety of molecular structures, the dopant amount used in EML, the cost of metal precursor, and the complexity of synthetic procedure may limit the Pt(II) and Os(II) complexes for the large-scale and versatile application on electronic devices. By comparison, the cyclometalated Ir(III) complexes possess their distinctive advantages (Chen et al., 2020b). The development of NIR OLEDs based on Ir(III) emitters has drawn increasing attention, and the enhancement of the EQE performance becomes a pressing demand. To realize the NIR-emitting Ir(III) complexes, the strategy of using the cyclometalated ligands with the extensively conjugated rings was used (Qiao et al., 2009). Even though the emission wavelengths are obviously red-shifted, the ^{3}MLCT contributions at the excited state manifolds of these Ir(III) complexes decreased and the increased π–π interactions between neighboring entities may cause a strong triplet-triplet annihilation (TTA) (Kim et al., 2020), resulting in the undesired decay to the ground states through nonradiative decays. While the use of the rigid and unitary cyclometalated ligands in the Ir(III) phosphors was recently studied, this method can restrict the intramolecular motion and was demonstrated to improve PLQYs of the designed Ir(III) complexes (You et al., 2020a); however, the intricate chemical structures and multistep synthesis steps may limit its practical application. Thus, using structurally simple and synthetically accessible Ir(III) emitters with less conjugated rings or complex groups should be the preferable entrance to get efficient NIR-emitting Ir(III) cyclometalated complexes, as the triplet excited states of these structurally simple Ir(III) phosphors can be strengthened, leading to restricted nonradiative processes, high PLQYs, and excellent EL performance.

The functional groups on the cyclometalated ligands can influence the optoelectronic properties of the Ir(III) complex (Kim et al., 2011), and the electron-withdrawing or electron-donating substituents play a different role on the regulation of emission wavelengths (Kim et al., 2018b; Zhou et al., 2008). For the systematic investigation on the methodology to readily tune the emission color from the DR to the NIR region (≥700 nm), three new heteroleptic Ir(III) phosphors with different functional groups including the electron-withdrawing cyano group, the electron-donating *tert*-butyl, and dimethyl groups added on the 1-phenylisoquinoline-4-carbonitrile cyclometalated ligand have been designed and synthesized. The data were compared with that of the parent complex Ir(piq-CN)$_2$(acac) (**CNIr**) (piq = 1-phenylisoquinoline) (Chen et al., 2020b). The results reveal that the introduction of CN group on the phenyl moiety will slightly blue-shift the emission spectrum; in contrast, the incorporation of *tert*-butyl and dimethyl groups exerts a bathochromic effect on the luminescence. The density functional theory (DFT) calculations have indicated that the CN group can significantly lift down both the lowest unoccupied molecular orbital (LUMO) and HOMO of the complex while the alkyl groups mainly elevate the HOMO energy level. It is also noted that the NIR OLEDs by using these easily available Ir(III) complexes can afford high-efficiency performances. The maximum EQE of 7.1% with the emission peak at 695 nm is achieved for the **Bu-CNIr**-based device. Especially, the maximum EQE of 7.2% with the emission peak at 714 nm is achieved for the **DM-CNIr**-based device, which is one of the most efficient Ir(III)-based NIR OLEDs to date (Cao et al., 2015; Kesarkar et al., 2016; Chen et al., 2018; Xue et al., 2017; Tao et al., 2013; You et al., 2019, 2020b; Fu et al., 2018; Zhou et al., 2019).

RESULTS AND DISCUSSION

Synthetic strategies and chemical characterization

Initial reactants such as 1-chloroisoquinoline-4-carbonitrile, 4-cyanophenylboronic acid, 4-*tert*-butylphenylboronic acid, and 3,5-dimethylphenylboronic acid are available from commercial sources, and all

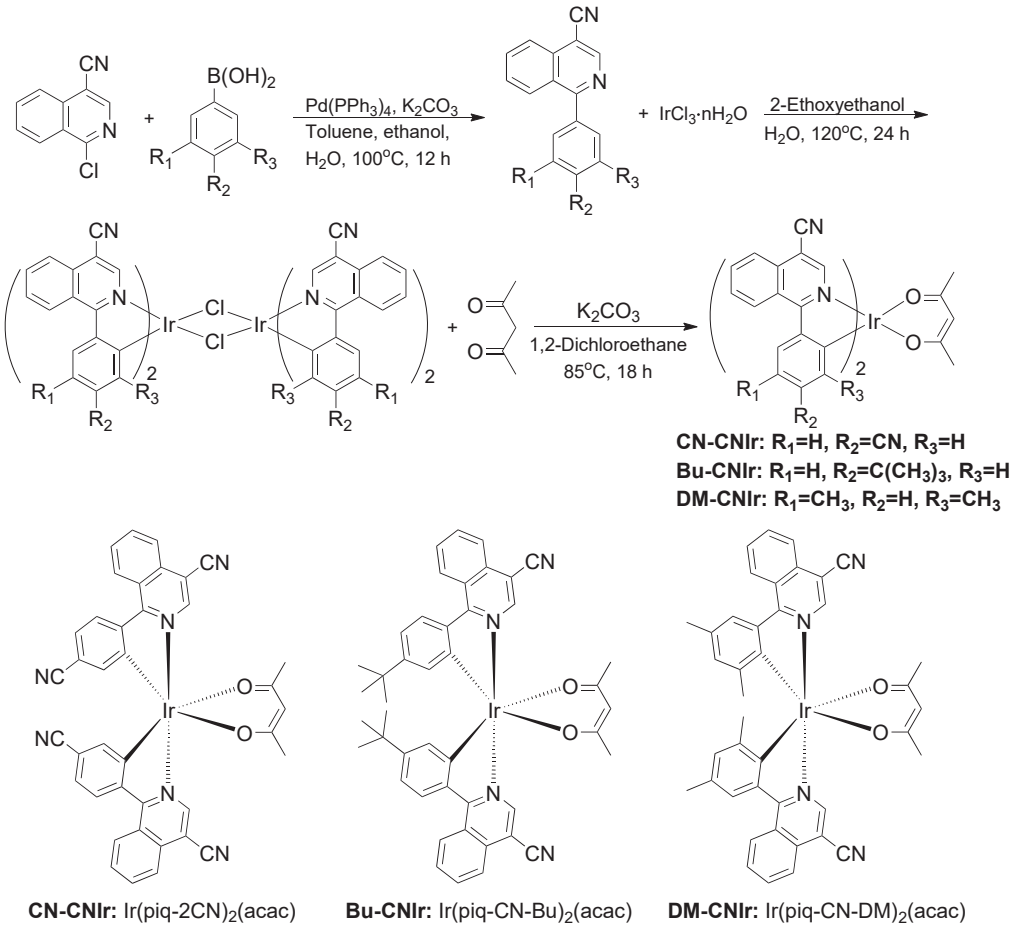

Scheme 1. The chemical structures and synthesis route of three DR-NIR-emitting Ir(III) phosphors

were used directly without further purification. Three cyclometalated ligands were synthesized via Suzuki coupling reaction (Scheme 1). Then, the reaction of cyclometalated ligands and $IrCl_3 \cdot 3H_2O$ furnished the corresponding μ-chlorobridged dimers. In the last step, the Ir(III) dimers were allowed to react with the ancillary ligand acetylacetone (acac) to obtain Ir(piq-2CN)$_2$acac (**CN-CNIr**), Ir(piq-CN-Bu)$_2$acac (**Bu-CNIr**), and Ir(piq-CN-DM)$_2$acac (**DM-CNIr**).

Single-crystal X-ray crystallography

The crystal structure of **CN-CNIr** was confirmed by the X-ray diffraction study (Figure 1) in which a tris-bidentate and six-coordinated structure is clearly shown. Single crystals of **CN-CNIr** were obtained by slowly diffusing petroleum ether into the dichloroethane solution of the Ir(III) complex. The relevant structural parameters of **CN-CNIr** reveal that the complex adopts a monoclinic crystal system (Table S1, ESI). Besides, the selected bond lengths and angles around the iridium center are summarized in Table S2 (ESI). The bond lengths between the metal center and the *phenyl*-C, *pyridyl*-N and *acac*-O in **CN-CNIr** are 1.958(8), 2.036(6), and 2.134(5) Å, respectively. The bond angle formed between the two *trans*-N and iridium atom is 176.8(3)°. Meanwhile, the crystal packing diagram reveals that the interactions of CN···H, CN···CN, O···H and so on are the main driving forces to maintain the packing order of the Ir(III) complex (Figure S16, ESI). The measured distance of H4···CN on the isoquinoline is ca. 2.513 Å, the distance of two adjacent CN groups is situated between ca. 2.469 and 2.595 Å, the distance of acac O1···H3 is ca. 2.692 Å, while the distances between CN on the phenyl moiety and H14 on the isoquinoline as well as H19a on the acac ligand are ca. 2.583 and 2.670 Å, respectively. The strong electron-withdrawing property of the cyano group can induce the intermolecular interactions in the aggregates of complexes (Li and Li, 2020).

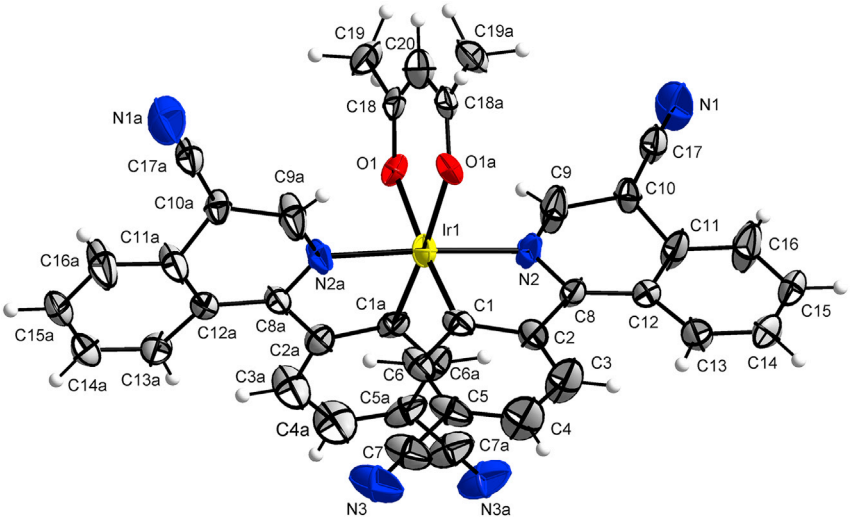

Figure 1. The crystal structure of CN-CNIr

Photophysical and thermal properties

The UV-vis absorption and photoluminescence (PL) spectra of three Ir(III) complexes in tetrahydrofuran (THF) at 298 K are presented in Figure 2. All the complexes show high-energy absorption bands in the wavelength region from 200 to 400 nm with larger molar extinction coefficients ($\varepsilon > 2.0 \times 10^4$ M^{-1} cm^{-1}), which can be assigned to the ligand-centered (LC) $\pi-\pi^*$ transition of cyclometalated C^N ligands. For the relatively weaker absorption bands beyond 400 nm, they are ascribed to the intramolecular charge transfer (ICT) transitions including the MLCT transition. **DM-CNIr** exhibits slightly stronger absorption than **CN-CNIr** and **Bu-CNIr**, which may be due to the transition state caused by the charge transfer (CT) from the electron-donating phenyl ring with two methyl substituent groups to the electron-withdrawing quinolone ring with CN moiety in the cyclometalated ligand. For the emission property, the three phosphors show PL peaks at 688, 700, and 709 nm, respectively, in THF solutions, corresponding to the DR-NIR region for **CN-CNIr** and the NIR region for **Bu-CNIr** and **DM-CNIr**. In comparison with the PL peak of the parent complex **CNIr** at 696 nm (Figure S17, Chen et al., 2020b), **CN-CNIr** presents a blue-shifted emission spectrum while both **Bu-CNIr** and **DM-CNIr** show red-shifted emission spectra. This illustrates that the introduction of electron-donating groups such as *tert*-butyl and dimethyl groups can elevate the HOMO levels, while incorporating electron-withdrawing group such as cyano group will lower the HOMO levels. Actually, incorporation of the cyano group in the phenyl moiety has a significant influence on both HOMO and LUMO energy levels, which also has been corroborated in the DFT calculations. The emission quantum yields (Φ_{em}) of these three DR-NIR-emitting Ir(III) complexes in CH_2Cl_2 solutions were measured with $Ir(piq)_2(acac)$

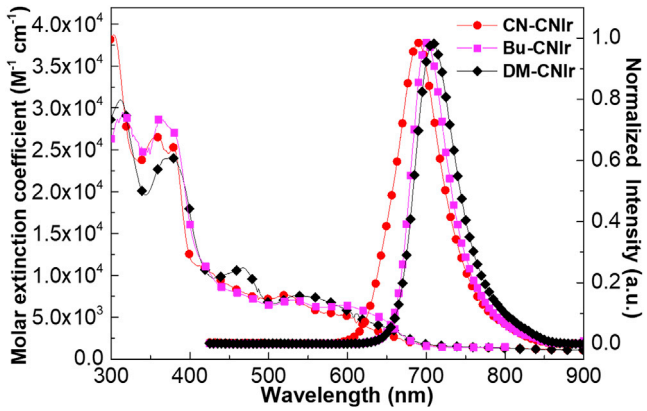

Figure 2. UV-vis absorption and PL spectra of the three DR-NIR-emitting Ir(III) phosphors in THF solutions at room temperature

Table 1. The summary of photophysical and thermal stability data of three DR-NIR-emitting Ir(III) complexes

Complex	λ_{abs} [a] (nm, 10^3 M^{-1} cm^{-1})	$\lambda_{PL,max}$ (nm)	Φ_{em}	τ_{em} (μs)	k_r [e] [10^5 s^{-1}]	k_{nr} [e] [10^6 s^{-1}]	T_{dec} [f] [°C]
CN-CNIr	303(38.7), 358(26.5), 379(25.3), 421(10.9), 521(7.6), 672(2.3)	688[a], 665[b]	0.08[c], 0.10[d]	0.24[c], 2.86[b]	3.3	3.8	198
Bu-CNIr	315(29.6), 366(28.8), 439(8.7), 534(7.1), 596(6.4), 657(3.9)	700[a], 674[b]	0.15[c], 0.17[d]	0.28[c], 3.10[b]	5.4	3.0	332
DM-CNIr	312(30.9), 376(24.1), 467(11.0), 537(7.6), 612(5.5), 672(2.9)	709[a], 686[b]	0.08[c], 0.17[d]	0.29[c], 3.74[b]	2.8	3.2	301

[a]Measured in THF solutions at room temperature.
[b]Measured in THF solutions at 77 K.
[c]Measured in CH_2Cl_2 solutions at room temperature. Φ_{em} was calculated by referencing the integrated emission intensity to that of **Ir(piq)$_2$(acac)** (Φ_{em} = 0.20).
[d]Measured in films (15 wt% phosphors in CBP) at room temperature.
[e]Calculated by the equations of $\Phi_{em} = k_r/(k_r + k_{nr})$ and $\tau_{em} = 1/(k_r + k_{nr})$ and these values are for solutions.
[f]Onset decomposition temperature at 5% degradation measured by thermogravimetric analysis.

(Φ_{em} = 0.20) as a standard (Su et al., 2003; Song et al., 2012; Brouwer 2011). The Φ_{em} of **CN-CNIr**, **Bu-CNIr,** and **DM-CNIr** are 0.08. 0.15, and 0.08, respectively. Meanwhile, their Φ_{em} in doped films (15 wt% phosphors in 4,4′-N,N′-dicarbazole-biphenyl [CBP]) were also recorded, increasing to 0.10, 0.17, and 0.17, compared with those of the solutions. In addition, the emission lifetimes (τ_{em}) of three Ir(III) phosphors at room temperature are almost comparable with each other (0.24–0.29 μs, Figure S18–S20), and at 77 K, these values were significantly raised to 2.86, 3.10, and 3.74 ms for **CN-CNIr**, **Bu-CNIr,** and **DM-CNIr**, respectively. Even though the calculated nonradiative decay rate constants (k_{nr}) are larger than the radiative rate constants (k_r) for the three DR-NIR-emitting Ir(III) phosphors (Table 1), the radiative transition has been enhanced compared with the other NIR-emitting Ir(III) emitters (Kesarkar et al., 2016; Chen et al., 2018; Xue et al., 2017; Tao et al., 2013; Fu et al., 2018) probably due to the fact that the introduction of the CN group would strengthen the triplet MLCT states of the whole complex. Moreover, the thermal properties of three Ir(III) complexes have been tested by thermogravimetric analysis (TGA) under a nitrogen flow (Figure S21). **Bu-CNIr** and **DM-CNIr** show good thermal stabilities with the decomposition temperatures at the 5% degradation of over 300°C.

Computational studies

DFT calculations were used to rationalize the spectral and electronic properties of three DR-NIR-emitting Ir(III) phosphors. As shown in Figure 3, the LUMOs of these complexes are mainly located on the isoquinoline and aromatic phenyl rings, while the HOMOs are mainly distributed on the aromatic phenyl rings and metal center. In consequence, the HOMO and LUMO of the complexes have a good overlap, and it results in a narrow E_g and a long-wavelength emission. The atomic contributions of the frontier orbitals (e.g. HOMO-4 to LUMO+4, LSOMO, and HSOMO) were computed, and the transition of frontier molecular orbitals in the triplet state indicates the emission arises from the ^{3}MLCT for these Ir(III) phosphors (Figures S22–S33, Tables S3–S8, ESI). To modulate the frontier orbitals by change of the cyclometalated ligand, the addition of electron-withdrawing CN group on the isoquinoline ring decreases the electron donation of the isoquinoline moiety to the iridium center, leading to a much lowered HOMO and LUMO of the Ir(III) complex. Then, when we introduce CN unit into the phenyl ring in **CN-CNIr**, both HOMO and LUMO energy levels would be further lifted down significantly. It seems that if the CN group is added in the isoquinoline moiety, there is a larger influence on LUMO than that on HOMO, while if the CN group is incorporated into the phenyl moiety, the calculations show that it plays a more substantial role on HOMO than that on LUMO, finally leading to a slightly broader energy gap E_g for **CN-CNIr** than for **CNIr**. Meanwhile, the functionalization of alkyl groups on the phenyl part makes the HOMO levels elevate more evidently. As a result, the emission peaks of **Bu-CNIr** and **DM-CNIr** in solutions can be extended to the NIR range (≥700 nm). In general, the introduction of the CN group on the isoquinoline moiety can make the E_g values of phosphors significantly decrease and move the emission range of Ir(III) complexes to the DR-NIR range. At the same time, the addition of CN group on the phenyl moiety would slightly blue shift the emission peak for **CN-CNIr**, but the addition of *tert*-butyl and methyl groups leads to the bathochromic effect for **Bu-CNIr** and **DM-CNIr**.

Electrochemical properties

The cyclic voltammetry (CV) was performed with ferrocene that acts as the internal standard under N_2 to investigate the electrochemical properties of three Ir(III) complexes (Figure 4). In the cathodic scan, all

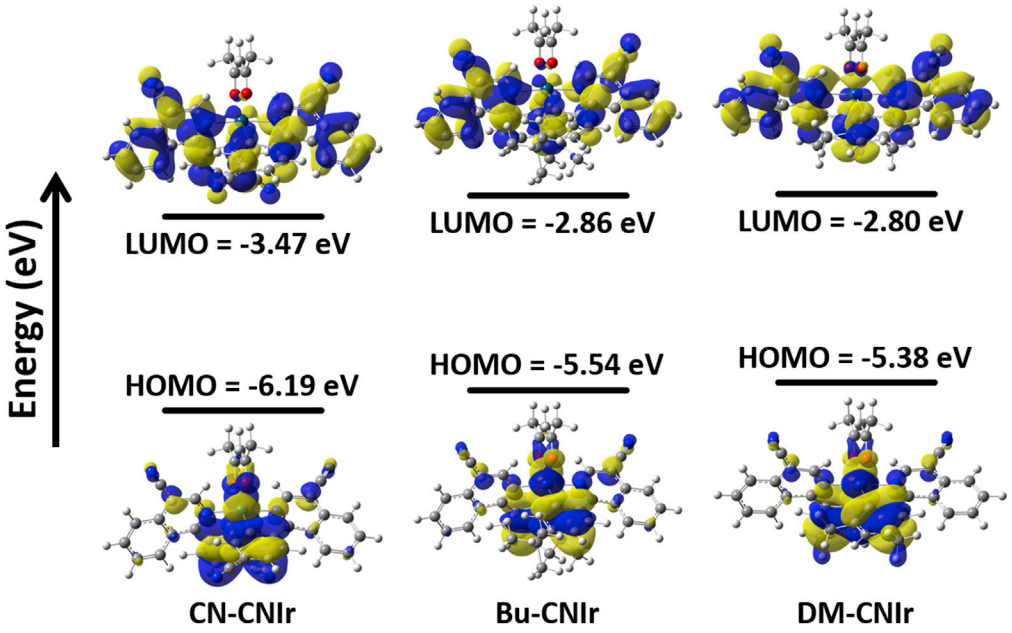

Figure 3. The calculated HOMO and LUMO energy levels of the three Ir(III) complexes

the complexes exhibit reduction waves with onset potentials (E_{re}) located between ca. −0.6 V and −1.6 V, which could be assigned to the reduction of the CN-quinolyl moiety in the cyclometalated ligand. Especially, the CN group in the phenyl ring could furnish an obviously lower reduction potential that is consistent with the relatively lower LUMO energy level of **CN-CNIr** than that of **Bu-CNIr** and **DM-CNIr**, which is correlated by the DFT calculations as well. On the other hand, oxidation waves have also been observed for this series of Ir(III) complexes. Three Ir(III) complexes show a decreasing trend on the oxidation potentials (from 0.72 V to 0.51 V *vs.* ferrocene), and this can be explained by the fact that the electron-withdrawing group, i.e., CN, can increase the electron deficiency at the *meta*-position ($C_{C\text{-}Ir}$), while the electron-donating groups, i.e., $C(CH_3)_3$, and a pair of CH_3 groups can increase the electron richness of the phenyl ring, resulting in the different degrees of electron donation from C^N ligand to the d orbitals of Ir(III) center of three complexes, hence leading to the gradually elevated HOMO levels. The HOMO and LUMO energy levels calculated by CV and DFT for **CN-CNIr**, **Bu-CNIr,** and **DM-CNIr** are summarized in Table 2.

Electroluminescent OLED performance

We chose **Bu-CNIr** and **DM-CNIr** as the emitters to explore their potentials for the NIR OLED applications. On account of the narrow E_g of these phosphors and deep HOMO of CBP (HOMO = −6.1 eV), CBP was chosen as the host material in the emissive layer (EML). The OLED device structures were fabricated as follows: indium tin oxide (ITO)/dipyrazino[2,3-*f*:2′,3′-*h*]quinoxaline-2,3,6,7,10,11-hexacarbonitrile (HAT-CN) (20 nm)/4,4′-(cyclohexane-1,1-diyl)bis(*N*,*N*-di-*p*-tolylaniline) (TAPC) (40 nm)/1,3-di(9*H*-carbazol-9-yl)benzene (mCP) (5 nm)/Ir (x wt%): CBP (30 nm)/1,3,5-tris[N-(phenyl)-benzimidazole]benzene (TPBi) (40 nm)/LiF (1 nm)/Al (100 nm) (Figure 5A). In the configuration of OLEDs, the hole flows from ITO. HAT-CN is utilized as the hole injection layer. TAPC and mCP both act as the hole transport layers, in which 5-nm mCP also plays the role of electron blocking. The Ir phosphors are doped in CBP. TPBi serves as the functional layer for both electron transporting and hole blocking, LiF acts as the electron injection layer, and the electron flows from Al. The electronic energy levels in the device are well matched and ensure the good performances of NIR OLEDs based on the emitters **Bu-CNIr** and **DM-CNIr** (Figure 5B).

Four OLED devices (**D1**-**D4**) were fabricated, in which **D1**-**D3** utilized **Bu-CNIr** as the emitter with increased doping concentrations (10, 15, and 20 wt%, respectively) while **D4** was based on **DM-CNIr** as the dopant emitter (15 wt%). The EL maxima of **D1**-**D3** are red-shifted from 693 to 700 nm as the doping concentration increases, and **D4** affords an emission peak at 714 nm (Figures 6A and S34A). After the turn-on voltage (V_{on} of 4.0–4.3 V for **D1**-**D4**, Figures 6B and S34B) was reached, the fabricated OLEDs based on the two Ir(III)

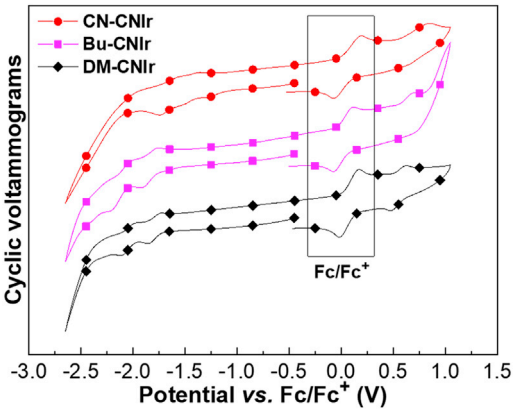

Figure 4. CV curves of three DR-NIR-emitting Ir(III) phosphors in CH_2Cl_2 solutions (The onset potentials of the oxidation wave of Fc/Fc^+ couple are plotted to occur at 0 V)

emitters displayed the NIR electroluminescence. Only the emission originated from the Ir(III) phosphor is detected in the devices, suggesting the inner confinement of the triplet excitons in the EML and the efficient energy transfer of excitons from the host to the metallophosphor dopant. High EQEs are achieved by using our designed **Bu-CNIr** and **DM-CNIr** as the emitters. For **D1**-**D3**, the increase of doping concentration in EML from 10 to 15 wt% does not induce the degradation of OLED performance. When the doping concentration is 20 wt%, the device is affected by the TTA and/or concentration self-quenching effect. The peak EQEs of 7.1, 7.1, and 5.5% are achieved for **D1**, **D2**, and **D3**, respectively. The EQEs can remain at 3.9, 3.9, and 3.6% at 500 cd m^{-2} (Figure S34C). The current densities ($J_{1/2}$) when the peak EQEs are dropped to their half values are recorded at 296, 316, and 555 mA cm^{-2} for the three devices, indicating the good EQE stabilities of OLEDs. The luminance at 14 V can be as high as 1413, 1410, and 1433 cd m^{-2} for **D1**-**D3** (Table 3). For **D4**, it attains a peak EQE of 7.2%, which is at the high level of reported Ir(III) complexes-based NIR-OLEDs (Figure S35). The EQE remains at 4.7% when the luminance is 100 cd m^{-2} (Figure 6C). A satisfactory current density ($J_{1/2}$) of 270 mA cm^{-2} is recorded when the maximum EQE is dropped to its half value (Table 3). Besides, a maximum luminance of 532 cd m^{-2} at 15 V is achieved. Each device shows a relatively low current efficiency (CE) and power efficiency (PE) (Figures 6D and S34D), which is a common observation in the Ir(III)-based NIR OLEDs and should be ascribed to the relatively low luminous intensity and luminous flux in the region of long wavelengths (especially from 700 to 780 nm). The operational stabilities of **D2** and **D4** are also tested with the initial luminance of 100 cd m^{-2}, and the operational lifetime values at 50% of the initial luminance (T_{50}) are 5.9 and 2.1 hr, respectively (Figure S36). Overall, this successful case facilitates the development of our simple design strategy (the addition of CN group) to attain efficient NIR-emitting Ir(III) phosphors. Besides, our study demonstrates that the structural modifications on the cyclometalated ligand of 1-phenylisoquinoline-4-carbonitrile are able to mediate the optoelectronic properties of the synthetic Ir(III) complexes. Especially, the introduction of the alkyl groups can promote the phosphorescence of OLEDs based on our designed Ir(III) complexes with high EQEs in the NIR range.

Table 2. The highest occupied molecular orbital (HOMO) and lowest unoccupied molecular orbital (LUMO) levels calculated by CV and DFT for three Ir(III) complexes

			E_g					
Complex	E_{ox} (V)[a]	E_{red} (V)[b]	E_g^{cv} (eV)[c]	E_g (eV)[d]	E_{HOMO} (eV)[e]	E_{LUMO} (eV)[f]	E_{HOMO} (eV)[d]	E_{LUMO} (eV)[d]
CN-CNIr	0.72	−1.18	1.90	2.72	−5.52	−3.62	−6.19	−3.47
Bu-CNIr	0.59	−1.76	2.35	2.68	−5.39	−3.04	−5.54	−2.86
DM-CNIr	0.51	−1.72	2.23	2.58	−5.31	−3.08	−5.38	−2.80

[a]The values were obtained from the onset potential of the first oxidation wave of the CV curves.
[b]The values were obtained from the onset potential of the first reduction wave of the CV curves.
[c]CV-derived energy gap E_g^{cv} calculated from the difference between HOMO and LUMO.
[d]Data obtained from DFT calculations.
[e]HOMO levels were calculated according to the equation HOMO = − (4.8 + E_{ox}) eV.
[f]LUMO levels were calculated according to the equation LUMO = − (4.8 + E_{red}) eV.

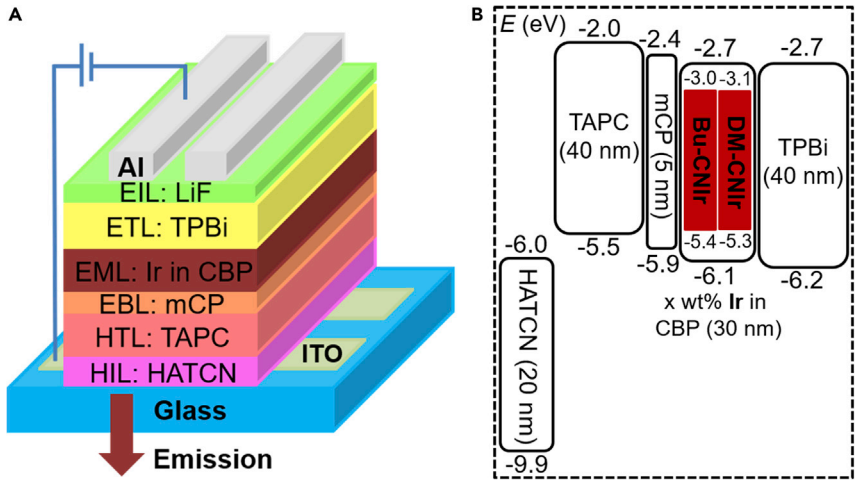

Figure 5. Device structure and energy level diagram of the materials for OLEDs

(A) Device structure of the OLED device.

(B) Energy level diagram of the OLED device.

Conclusions

By using the structurally simple and accessible 1-phenylisoquinoline-4-carbonitrile derivatives as the cyclometalated ligands, three newly designed DR-NIR-emitting Ir(III) complexes **CN-CNIr**, **Bu-CNIr**, and **DM-CNIr** were synthesized and investigated. The optoelectronic properties of Ir(III) complexes can be modulated by the structural functionalization of cyclometalated ligands. Specifically, both the HOMO and LUMO levels of the Ir(III) complex are lowered by introducing the CN group in the phenyl moiety, while incorporating the alkyl groups in the phenyl ring mainly elevates the HOMO level. The OLEDs based on **Bu-CNIr** afford a maximum EQE of 7.1% with the EL peak at 695 nm, and the device based on **DM-CNIr** displays a good performance in the NIR region and a maximum EQE of 7.2% with the EL

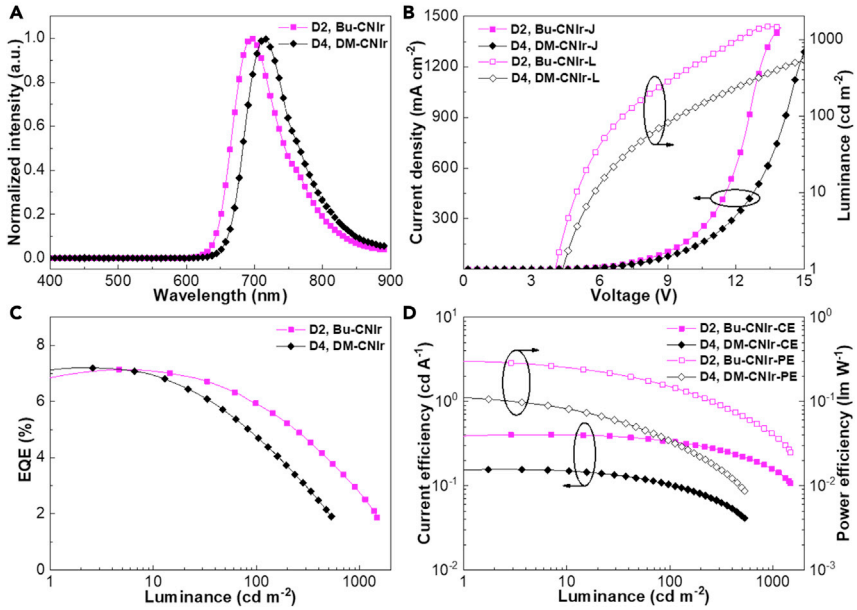

Figure 6. The performance of OLED devices based on Bu-CNIr and DM-CNIr

(A) Electroluminescence spectra.

(B) Current density-voltage-luminance (*J-V-L*) curves.

(C) EQE-current density curves.

(D) Curves of CE and PE versus current density.

Table 3. The EL performance of OLED devices using phosphors Bu-CNIr and DM-CNIr as the emitters

Device	Emitter (x wt%)	V_{on}[a] [V]	λ_{max} [nm]	EQE [%]	L [cd m^{-2}]	$J_{1/2}$[g] [mA cm^{-2}]
D1	Bu-CNIr (10)	4.1	693	7.1[b], 5.9[c], 3.9[d]	1413[e]	296
D2	Bu-CNIr (15)	4.0	695	7.1[b], 5.9[c], 3.9[d]	1410[e]	316
D3	Bu-CNIr (20)	4.1	700	5.5[b], 5.0[c], 3.6[d]	1433[e]	555
D4	DM-CNIr (15)	4.3	714	7.2[b], 4.7[c], 2.0[d]	532[f]	270

[a]The turn-on voltage (V_{on}) at the luminance of 1 cd m^{-2}.
[b]The peak EQE.
[c]The EQE at the luminance of 100 cd m^{-2}.
[d]The EQE at the luminance of 500 cd m^{-2}.
[e]The luminance at 14 V.
[f]The luminance at 15 V.
[g]The current density when the EQE was dropped to its half value.

peak at 714 nm. The present study reconfirms our successful design strategy for achieving the efficient NIR-emitting Ir(III) phosphors.

Limitations of the study

It is still a challenge to restrain the nonradiative decay upon narrowing the energy gap between the lowest excited state (S_1 or T_1) and the ground state (S_0).

STAR★METHODS

Detailed methods are provided in the online version of this paper and include the following:

- KEY RESOURCES TABLE
- RESOURCE AVAILABILITY
  - Lead contact
  - Material availability
  - Data and code availability
- METHODS DETAILS
  - Experimental section
  - X-ray crystallography
  - Computational details
  - OLED fabrication and measurements
  - General procedure for the syntheses of the ligands
  - General procedure for the syntheses of the iridium(III) complexes
- QUANTIFICATION AND STATISTICAL ANALYSIS

SUPPLEMENTAL INFORMATION

Supplemental information can be found online at https://doi.org/10.1016/j.isci.2021.102911.

ACKNOWLEDGMENTS

W.-Y.W. thanks the National Natural Science Foundation of China (51873176), Hong Kong Research Grants Council (PolyU153058/19P), Hong Kong Polytechnic University (1-ZE1C), Research Institute for Smart Energy (RISE), and the Endowed Professorship in Energy from Ms Clarea Au (847S) for the financial support.

AUTHOR CONTRIBUTIONS

H.Z., Z.C., R.L., and W.-Y.W. conceived this strategy and launched this project. H.Z. synthesized all the materials and conducted experimental characterizations. Y.X. carried out the DFT calculations and analyzed these data. H.Z., Z.C., and S.C. fabricated the OLED devices and tested their performances. H.Z., R.L., and W.-Y.W. wrote and revised the manuscript with assistance from all other coauthors. All authors have given approval to the final version of the manuscript.

DECLARATION OF INTERESTS

The authors declare no competing interests.

W.-Y.W. is a Guest Editor on Near-infrared (NIR) Luminescent Materials Special Issue published in iScience.
W.-Y.W. is also the editorial advisory board member of iScience.

Received: February 14, 2021
Revised: June 2, 2021
Accepted: July 23, 2021
Published: August 20, 2021

REFERENCES

Abdurahman, R., Yang, C., and Yan, X. (2016). Conjugation of a photosensitizer to near infrared light renewable persistent luminescence nanoparticles for photodynamic therapy. Chem. Commun. *52*, 13303–13306.

Ai, X., Evans, E.W., Dong, S., Gillett, A.J., Guo, H., Chen, Y., Hele, T.J.H., Friend, R.H., and Li, F. (2018). Efficient radical-based light-emitting diodes with doublet emission. Nature *563*, 536–540.

Baride, A., Meruga, J., Douma, C., Langerman, D., Crawford, G., Kellar, J.J., Cross, W.M., and May, P.S. (2015). A NIR-to-NIR upconversion luminescence system for security printing applications. RSC Adv. *5*, 101338–101346.

Brouwer, A.M. (2011). Standards for photoluminescence quantum yield measurements in solution (IUPAC Technical Report). Pure Appl. Chem. *83*, 2213–2228.

Bunzli, J.G., and Eliseeva, S.V. (2010). Lanthanide NIR luminescence for telecommunications, bioanalyses and solar energy conversion. J. Rare Earths *28*, 824–842.

Cao, X., Miao, J., Zhu, M., Zhong, C., Yang, C., Wu, H., Qin, J., and Cao, Y. (2015). Near-infrared polymer light-emitting diodes with high efficiency and low efficiency roll-off by using solution-processed iridium(III) phosphors. Chem. Mater. *27*, 96–104.

Chen, Z., Wang, L., Ho, C., Chen, S., Suramitr, S., Plucksacholatarn, A., Zhu, N., Hannongbua, S., and Wong, W.-Y. (2018). Smart design on the cyclometalated ligands of iridium(III) complexes for facile tuning of phosphorescence color spanning from deep-blue to near-infrared. Adv. Opt. Mater. *6*, 1800824.

Chen, J., Tao, W., Chen, W., Xiao, Y., Wang, K., Cao, C., Yu, J., Li, S., Geng, F., Adachi, C., et al. (2019). Red/near-infrared thermally activated delayed fluorescence OLEDs with near 100 % internal quantum efficiency. Angew. Chem. Int. Ed. *58*, 14660–14665.

Chen, W., Sukpattanacharoen, C., Chan, W., Huang, C., Hsu, H., Shen, D., Hung, W., Kungwan, N., Escudero, D., Lee, C., et al. (2020a). Modulation of solid-state aggregation of square-planar Pt(II) based emitters: enabling highly efficient deep-red/near infrared electroluminescence. Adv. Funct. Mater. *30*, 2002494.

Chen, Z., Zhang, H., Wen, D., Wu, W., Zeng, Q., Chen, S., and Wong, W.-Y. (2020b). A simple and efficient approach toward deep-red to near-infrared-emitting iridium(III) complexes for organic light-emitting diodes with external quantum efficiencies of over 10%. Chem. Sci. *11*, 2342–2349.

Chen, Z., Suramitr, S., Zhu, N., Ho, C.-L., Hannongbua, S., Chen, S., and Wong, W.-Y. (2020c). Tetrafluorinated phenylpyridine based heteroleptic iridium(III) complexes for efficient sky blue phosphorescent organic light-emitting diodes. J. Mater. Chem. C *8*, 2551–2557.

Dolomanov, O.V., Bourhis, L.J., Gildea, R.J., Howard, J.A.K., and Puschmann, H. (2009). OLEX2: a complete structure solution, refinement and analysis program. J. Appl. Crystallogr. *42*, 339–341.

Der Ende, B.M., Aarts, L., and Meijerink, A. (2009). Near-infrared quantum cutting for photovoltaics. Adv. Mater. *21*, 3073–3077.

Frisch, M.J., Trucks, G.W., Schlegel, H.B., Scuseria, G.E., Robb, M.A., Cheeseman, J.R., Scalmani, G., Barone, V., Petersson, G.A., Nakatsuji, H., et al. (2009). Gaussian 09, Revision D.01 (Gaussian, Inc.).

Fu, G., Zheng, H., He, Y., Li, W., Lu, X., and He, H. (2018). Efficient near-infrared (NIR) polymer light-emitting diodes (PLEDs) based on heteroleptic iridium(III) complexes with post-modification effects of intramolecular hydrogen bonding or BF_2-chelation. J. Mater. Chem. C *6*, 10589–10596.

Kesarkar, S., Mróz, W., Penconi, M., Pasini, M., Destri, S., Cazzaniga, M., Ceresoli, D., Mussini, P.R., Baldoli, C., Giovanella, U., et al. (2016). Near-IR emitting iridium(III) complexes with heteroaromatic β-diketonate ancillary ligands for efficient solution-processed OLEDs: structure–property correlations. Angew. Chem. Int. Ed. *55*, 2714–2718.

Kim, D.H., Cho, N.S., Oh, H.-Y., Yang, J.H., Jeon, W.S., Park, J.S., Suh, M.C., and Kwon, J.H. (2011). Highly efficient red phosphorescent dopants in organic light-emitting devices. Adv. Mater. *23*, 2721–2726.

Kim, D.H., Daleo, A., Chen, X., Sandanayaka, A.D., Yao, D., Zhao, L., Komino, T., Zaborova, E., Canard, G., Tsuchiya, Y., et al. (2018a). High-efficiency electroluminescence and amplified spontaneous emission from a thermally activated delayed fluorescent near-infrared emitter. Nat. Photon. *12*, 98–104.

Kim, H.U., Sohn, S., Choi, W., Kim, M., Ryu, S.U., Park, T., Jung, S., and Bejoymohandas, K.S. (2018b). Substituents engineered deep-red to near-infrared phosphorescence from tris-heteroleptic iridium(III) complexes for solution processable red-NIR organic light-emitting diodes. J. Mater. Chem. C *6*, 10640–10658.

Kim, H.U., Jang, H.J., Choi, W., Park, S., Park, T., Lee, J.Y., and Bejoymohandas, K.S. (2020). Aggregation-induced phosphorescence enhancement in deep-red and near-infrared emissive iridium(III) complexes for solution-processable OLEDs. J. Mater. Chem. C *8*, 4789–4800.

Kratzert, D., Holstein, J.J., and Krossing, I. (2015). DSR: enhanced modelling and refinement of disordered structures with SHELXL. J. Appl. Crystallogr. *48*, 933–938.

Kumar, P., Singh, S., and Gupta, B.K. (2016). Future prospects of luminescent nanomaterial based security inks: from synthesis to anti-counterfeiting applications. Nanoscale *8*, 14297–14340.

Li, Q., and Li, Z. (2020). Molecular packing: another key point for the performance of organic and polymeric optoelectronic materials. Acc. Chem. Res. *53*, 962–973.

Li, X., Lovell, J.F., Yoon, J., and Chen, X. (2020a). Clinical development and potential of photothermal and photodynamic therapies for cancer. Nat. Rev. Clin. Oncol. *17*, 657–674.

Li, X., Li, X., and Ma, H. (2020b). A near-infrared fluorescent probe reveals decreased mitochondrial polarity during mitophagy. Chem. Sci. *11*, 1617–1622.

Liao, J., Chi, Y., Yeh, C., Kao, H., Chang, C., Fox, M.A., Low, P.J., and Lee, G. (2015). Near infrared-emitting tris-bidentate Os(II) phosphors: control of excited state characteristics and fabrication of OLEDs. J. Mater. Chem. C *3*, 4910–4920.

Ly, K.T., Chen-Cheng, R.-W., Lin, H.-W., Shiau, Y.-J., Liu, S.-H., Chou, P.-T., Tsao, C.-S., Huang, Y.-C., and Chi, Y. (2017). Near-infrared organic light-emitting diodes with very high external quantum efficiency and radiance. Nat. Photon. *11*, 63–68.

Maldiney, T., Bessiere, A., Seguin, J., Teston, E., Sharma, S.K., Viana, B., Bos, A.J.J., Dorenbos, P., Bessodes, M., Gourier, D., et al. (2014). The in vivo activation of persistent nanophosphors for

optical imaging of vascularization, tumours and grafted cells. Nat. Mater. *13*, 418–426.

Mao, B., Chuang, C.H., Mccleese, C., Zhu, J., and Burda, C. (2014). Near-infrared emitting AgInS2/ZnS nanocrystals. J. Phys. Chem. C *118*, 13883–13889.

Peng, Q., Obolda, A., Zhang, M., and Li, F. (2015). Organic light-emitting diodes using a neutral π radical as emitter: the emission from a doublet. Angew. Chem. Int. Ed. *54*, 7091–7095.

Pichaandi, J., and Van Veggel, F.C. (2014). Near-infrared emitting quantum dots: recent progress on their synthesis and characterization. Coord. Chem. Rev. *263–264*, 138–150.

Qian, G., and Wang, Z.Y. (2010). Near-infrared organic compounds and emerging applications. Chem. Asian J. *5*, 1006–1029.

Qiao, J., Duan, L., Tang, L., He, L., Wang, L., and Qiu, Y. (2009). High-efficiency orange to near-infrared emissions from bis-cyclometalated iridium complexes with phenyl-benzoquinoline isomers as ligands. J. Mater. Chem. *19*, 6573–6580.

Richards, B.S. (2006). Luminescent layers for enhanced silicon solar cell performance: down-conversion. Sol. Energy Mater. Sol. Cells *90*, 1189–1207.

Song, M., Park, J.S., Gal, Y.-S., Kang, S., Lee, J.Y., Lee, J.W., and Jin, S.-H. (2012). Homologous series of phenylquinoline-carbazole main ligand based on red-emitting iridium(III) complexes for phosphorescent organic light-emitting diodes. J. Phys. Chem. C *116*, 7526–7533.

Su, Y.-J., Huang, H.-L., Li, C.-L., Chien, C.-H., Tao, Y.-T., Chou, P.-T., Datta, S., and Liu, R.-S. (2003). Highly efficient red electrophosphorescent devices based on iridium isoquinoline complexes: remarkable external quantum efficiency over a wide range of current. Adv. Mater. *15*, 884–888.

Tao, R., Qiao, J., Zhang, G., Duan, L., Chen, C., Wang, L., and Qiu, Y. (2013). High-efficiency near-infrared organic light-emitting devices based on an iridium complex with negligible efficiency roll-off. J. Mater. Chem. C *1*, 6446–6454.

Wang, X., Cui, L., Zhou, N., Zhu, W., Wang, R., Qian, X., and Xu, Y. (2013). A highly selective and sensitive near-infrared fluorescence probe for arylamine N-acetyltransferase 2 in vitro and in vivo. Chem. Sci. *4*, 2936–2940.

Wang, J., Ma, Q., Wang, Y., Shen, H., and Yuan, Q. (2017). Recent progress in biomedical applications of persistent luminescence nanoparticles. Nanoscale *9*, 6204–6218.

Wang, S.F., Yuan, Y., Wei, Y., Chan, W., Fu, L., Su, B., Chen, I., Chou, K., Chen, P., Hsu, H., et al. (2020). Highly efficient near-infrared electroluminescence up to 800 nm using platinum(II) phosphors. Adv. Funct. Mater. *30*, 2002173.

Xiang, H., Cheng, J., Ma, X., Zhou, X., and Chruma, J.J. (2013). Near-infrared phosphorescence: materials and applications. Chem. Soc. Rev. *42*, 6128–6185.

Xue, J., Xin, L., Hou, J., Duan, L., Wang, R., Wei, Y., and Qiao, J. (2017). Homoleptic facial Ir(III) complexes via facile synthesis for high-efficiency and low-roll-off near-infrared organic light-emitting diodes over 750 nm. Chem. Mater. *29*, 4775–4782.

Xue, J., Liang, Q., Wang, R., Hou, J., Li, W., Peng, Q., Shuai, Z., and Qiao, J. (2019). Highly efficient thermally activated delayed fluorescence via J-aggregates with strong intermolecular charge transfer. Adv. Mater. *31*, 1808242.

You, C., Liu, D., Meng, F., Wang, Y., Yu, J., Wang, S., Su, S., and Zhu, W. (2019). Iridium(III) phosphors with rigid fused-heterocyclic chelating architectures for efficient deep-red/near-infrared emissions in polymer light-emitting diodes. J. Mater. Chem. C *7*, 10961–10971.

You, C., Liu, D., Yu, J., Tan, H., Zhu, M., Zhang, B., Liu, Y., Wang, Y., and Zhu, W. (2020a). Boosting efficiency of near-infrared emitting iridium(III) phosphors by administrating their π–π conjugation effect of core–shell structure in solution-processed OLEDs. Adv. Opt. Mater. *8*, 2000154.

You, C., Liu, D., Zhu, M., Yu, J., Zhang, B., Liu, Y., Wang, Y., and Zhu, W. (2020b). σ–π and p–π conjugation induced NIR-emitting iridium(III) complexes anchored by flexible side chains in a rigid dibenzo[a,c]phenazine moiety and their application in highly efficient solution-processable NIR-emitting devices. J. Mater. Chem. C *8*, 7079–7088.

Yuan, Y., Liao, J., Ni, S., Jen, A.K., Lee, C., and Chi, Y. (2020). Boosting efficiency of near-infrared organic light-emitting diodes with Os(II)-based pyrazinyl azolate emitters. Adv. Funct. Mater. *30*, 1906738.

Zampetti, A., Minotto, A., and Cacialli, F. (2019). Near-infrared (NIR) organic light-emitting diodes (OLEDs): Challenges and Opportunities. Adv. Funct. Mater. *29*, 1807623.

Zhang, Y., Ran, Q., Wang, Q., Liu, Y., Hänisch, C., Reineke, S., Fan, J., and Liao, L. (2019). High-efficiency red organic light-emitting diodes with external quantum efficiency close to 30% based on a novel thermally activated delayed fluorescence emitter. Adv. Mater. *31*, 1902368.

Zhou, G., Ho, C.-L., Wong, W.-Y., Wang, Q., Ma, D., Wang, L., Lin, Z., Marder, T.B., and Beeby, A. (2008). Manipulating charge-transfer character with electron-withdrawing main-group moieties for the color tuning of iridium electrophosphors. Adv. Funct. Mater. *18*, 499–511.

Zhou, J., Fu, G., He, Y., Ma, L., Li, W., Feng, W., and Lü, X. (2019). Efficient and low-efficiency-roll-off near-infrared (NIR) polymer light-emitting diodes (PLEDs) based on an asymmetric binuclear iridium(III)-complex. J. Lumin. *209*, 427–434.

STAR★METHODS

KEY RESOURCES TABLE

REAGENT or RESOURCE	SOURCE	IDENTIFIER
Chemicals, peptides, and recombinant proteins		
1-Chloroisoquinoline-4-carbonitrile	Energy	CAS: 53,491-80-8
4-Cyanophenylboronic acid	Energy	CAS: 126747-14-6
4-*Tert*-butylphenylboronic acid	Energy	CAS: 123324-71-0
3,5-Dimethylphenylboronic acid	Energy	CAS: 172975-69-8
Acetylacetone	Energy	CAS: 123-54-6
Tetrakis(triphenylphosphane)palladium(0)	Heraeus	CAS: 14,221-01-3
Iridium(III) chloride hydrate	Heraeus	CAS: 14,996-61-3
Potassium carbonate	Dieckmann	CAS: 584-08-7
Deposited data		
Structure of CN-CNIr	This paper; Cambridge Crystallographic Data Center	CCDC: 2026717
Software and algorithms		
MestReNova	Mestrelab Research S. L.	https://mestrelab.com/software/mnova/
Gaussian 09	Frish et al., 2009	https://Gaussian.com
CrysAlisPRO	Agilent Technologies	https://rigaku.com/products/crystallography/crysalis
Olex2	OlexSys	https://www.olexsys.org/olex2/
SHELXL	George Sheldrick	http://shelx.uni-goettingen.de/
ChemDraw	PerkinElmer	https://www.perkinelmer.com/category/chemdraw
Other		
Ocean optics USB 2000 fiber Optic spectrometer	Ocean Optics, Inc.	https://www.oceaninsight.com/
Dual-channel Keithley 2614B source measure unit	Tektronix, Inc.	https://www.tek.com/keithley-source-measure-units/
PIN-25D Visible light silicon photodiode	OSI Optoelectronics	https://osioptoelectronics.com/

RESOURCE AVAILABILITY

Lead contact

Further information and requests for resources and reagents should be directed to and will be fulfilled by the lead contact, Wai-Yeung Wong (wai-yeung.wong@polyu.edu.hk).

Material availability

All new reagents generated in this study are available from the lead contact with a completed Materials Transfer Agreement.

Data and code availability

Crystallographic data for the structure reported in this paper have been deposited at the Cambridge Crystallographic Data Center (CCDC) and allocated with the deposition number CCDC 2026717. The published article includes all other datasets generated or analyzed during the study.

METHODS DETAILS

Experimental section

All commercially available starting materials were used directly with no further purification. The solvents were dried prior to use. All the reactions were carried out under an atmosphere of N_2 using standard

Schlenk techniques and were monitored by thin-layer chromatography (TLC) using Merck precoated aluminum sheets. Flash column chromatography was performed using silica gel purchased from Qingdao Haiyang Co., Ltd. Purification of the products was achieved *via* silica column chromatography with hexane/dichloromethane or hexane/ethyl acetate mixed solvents as eluents. Compounds were visualized under UV light irradiation at 254 or 365 nm. ^{1}H nuclear magnetic resonance (NMR) and ^{13}C NMR spectra were recorded in $CDCl_3$ solvent on a Bruker Avance 400 MHz spectrometer, which were calibrated using residual nondeuterated solvent peaks as an internal reference. The chemical shifts (δ) are reported in ppm, and the coupling constants (J) are expressed in Hertz (Hz). Mass spectra were obtained on a Bruker Autoflex matrix-assisted laser desorption ionization time-of-flight mass spectrometer (MALDI-TOF MS). TGA data were collected on a PerkinElmer TGA thermal analyzer under a N_2 atmosphere with a heating rate of 10°C/min. The UV-vis absorption spectra of Ir(III) complexes were measured on the Cary UV-300 spectrophotometer at room temperature using the quartz cuvette as the holder. Thermo Scientific Lumina fluorescence spectrometer was used to detect the PL spectra. The luminescence lifetimes were measured on a Horiba Deltaflex modular fluorescence lifetime system at room temperature, and the PL decay curves were fitted by using a single-exponential function $I(t) = A\exp(-t/\tau) + B$, where $I(t)$ is the intensity of light at time t, t is the time, and τ is the luminescence lifetime. The emission quantum efficiencies (Φ_{em}) were estimated by referencing the integrated emission intensity to that of $Ir(piq)_2(acac)$ ($\Phi_{em} = 0.20$) (Su et al., 2003; Song et al., 2012) using the equation: $\Phi_s = \Phi_r (n_s^2 D_s A_r / n_r^2 D_r A_s)$, where A_r and A_s (~0.1) are the absorbance of the reference and sample at 450 nm, D_r and D_s represent the integrated areas of the emission peaks of the reference and sample upon excitation at 450 nm, and n_r and n_s are the refractive indexes of the reference and sample solvents, respectively, where both of the solvents used are CH_2Cl_2 (Brouwer 2011; Chen et al., 2020c). The Ir(III) complexes were subjected to the electrochemical tests for CV on the CH Instruments CHI800D Serials electrochemical analyzer via a setup of three electrode system (working electrode: glassy carbon disk, reference electrode: Ag/AgCl immersed in saturated potassium chloride solution before use, counter electrode: Pt wire). The redox couple of ferrocene/ferrocenium (Fc/Fc^+) was used as the internal standard. The electrolyte is a dichloromethane solution of 0.1 M $[Bu_4N]PF_6$ and was degassed with nitrogen. In addition, all CV measurements were performed under a N_2 atmosphere.

X-ray crystallography

The crystal data of **CN-CNIr** were collected at 100 K on a Rigaku Oxford Diffraction Supernova Dual Source, Cu at Zero equipped with an AtlasS2 CCD using Cu Kα radiation. Data reduction was carried out using the diffractometer's software (Agilent Technologies, CrysAlisPRO, version, 2013). The structures were solved by direct methods using Olex2 software (Dolomanov et al., 2009), and the nonhydrogen atoms were located from the trial structure and refined anisotropically with SHELXL-2018 (Kratzert et al., 2015) using a full-matrix least squares procedure based on F^2. The weighted R factor, wR, and goodness-of-fit S values were obtained based on F^2. The hydrogen (H) atom positions were fixed geometrically at the calculated distances and allowed to ride on their parent atoms.

Computational details

For DFT calculations, the structures of these Ir(III) complexes were optimized by using DFT with the PBE0 functional. The LanL2DZ basis set and LanL2DZ pseudopotential were used for the iridium atom and the 6-31G(d) basis set for all other atoms. Frontier molecular orbitals (HOMO and LUMO) were calculated at B3PW91 level, using SDD basis set and SDD pseudopotential to treat the iridium atom and def2TZVP basis set to treat all other atoms. All the calculations were performed using the software package Gaussian 09 (Revision D.01, Frisch et al., 2009).

OLED fabrication and measurements

The layers of HAT-CN (20 nm)/TAPC (40 nm)/mCP (5 nm)/phosphor doped in CBP (10 wt%, 30 nm)/TPBi (40 nm)/LiF (1 nm)/Al (100 nm) were successively deposited on the precleaned ITO glass substrates at a pressure of less than 10^{-6} Torr. For each device, four pixels with the same device configuration were prepared at one batch, and the deposited Al cathode overlaps with the precoated ITO anode to afford an active area of 2 mm × 2 mm for each pixel. The EL spectra of devices were measured using the fiber optic spectrometer (Ocean Optics USB, 2000) in the normal direction. The J-V-L curves were investigated using a dual-channel Keithley 2614B source measure unit and a PIN-25D silicon photodiode.

General procedure for the syntheses of the ligands

For the cyclometalated C^N ligands, the corresponding phenyl boronic acid (1.0 equiv) and 1-chloroisoquinoline-4-carbonitrile (1.1 equiv) were added into a mixed solvent of toluene, EtOH, and H_2O (7:1:2, v/v/v) under a N_2 atmosphere. Then, $Pd(PPh_3)_4$ (0.05 equiv) and K_2CO_3 (2.0 equiv) were added into the reaction system. The reaction was allowed to proceed at 100°C for 18 hr. After cooling to room temperature, the mixture was diluted by 100 mL of ethyl acetate and washed with water. The collected organic solvent was removed under the reduced pressure followed by purification using the chromatography of silica gel column eluting with mixed PE/EA (5/1) to furnish the corresponding C^N ligands.

General procedure for the syntheses of the iridium(III) complexes

Under a N_2 atmosphere, the corresponding C^N ligand (2.2 equiv) and $IrCl_3 \cdot nH_2O$ (1.0 equiv, 60 wt % Ir content) were reacted in a mixture of 2-methoxyethanol and water (3:1, v/v) at 110°C for 24 hr. Then, the reaction mixture was cooled to room temperature and deionized water was added to precipitate the Ir(III) μ-chloro-bridged dimer. The solid was filtrated, collected and dried under vacuum. Without further purification, the Ir(III) μ-chloro-bridged dimer, acetylacetone (5.0 equiv) and Na_2CO_3 (10.0 equiv) were added into dichloroethene and the mixture was heated to 85°C overnight. After cooling to room temperature, the mixture was filtered by Celite and the organic layer was removed under the reduced pressure. The crude product was purified on a silica gel column using PE/EA (3/1) as eluent to give the corresponding pure Ir(III) complexes.

QUANTIFICATION AND STATISTICAL ANALYSIS

1-(4-Cyanophenyl)isoquinoline-4-carbonitrile (Piq-2CN). (yield, 50%) ^{1}H NMR (400 MHz, $CDCl_3$) δ 9.00 (1 H, s), 8.31 (1 H, d, J 8.3), 8.11 (1 H, d, J 8.5), 7.98 (1 H, d, J 1.2), 7.86 (4 H, td, J 8.5, 6.4), 7.76 (1 H, s). ^{13}C NMR (101 MHz, $CDCl_3$) δ 162.59, 147.55, 142.59, 135.88, 133.12, 132.55, 130.90, 129.76, 127.76, 125.68, 125.07, 118.44, 116.06, 113.73, 106.03. MS (MALDI-TOF) [m/z]: found $[M + H]^+$ 256.0844, calculated 255.0796 ($C_{17}H_9N_3$).

1-(4-*Tert*-butylphenyl)isoquinoline-4-carbonitrile (Piq-CN-Bu). (yield, 67%) ^{1}H NMR (400 MHz, $CDCl_3$) δ 8.95 (1 H, s), 8.30 (1 H, d, J 8.5), 8.25 (1 H, d, J 8.3), 7.91 (1 H, ddd, J 8.3, 7.0, 1.1), 7.76–7.64 (3 H, m), 7.62–7.42 (2 H, m), 1.40 (9 H, s). ^{13}C NMR (101 MHz, $CDCl_3$) δ 165.04, 153.24, 147.71, 135.79, 135.45, 132.54, 129.98, 128.93, 125.90, 125.74, 124.61, 116.58, 104.56, 35.00, 31.40. MS (MALDI-TOF) [m/z]: found $[M + H]^+$ 287.0030, calculated 286.1470 ($C_{20}H_{18}N_2$).

1-(3,5-Dimethylphenyl)isoquinoline-4-carbonitrile (piq-CN-DM). (yield, 62%) ^{1}H NMR (400 MHz, $CDCl_3$) δ 8.95 (1 H, s), 8.29–8.21 (2 H, m), 7.92 (1 H, ddd, J 8.1, 6.9, 1.2), 7.70 (1 H, ddd, J 8.5, 7.0, 1.2), 7.30 (2 H, m), 7.20 (1 H, s), 2.43 (6 H, d, J 0.8). ^{13}C NMR (101 MHz, $CDCl_3$) δ 165.48, 147.66, 138.42, 138.26, 135.74, 132.59, 131.52, 128.98, 128.97, 127.87, 126.03, 124.61, 116.57, 104.74, 21.51. MS (MALDI-TOF) [m/z]: found $[M + H]^+$ 259.0741, calculated 258.1157 ($C_{18}H_{14}N_2$).

CN-CNIr (black, yield: 12%) ^{1}H NMR (400 MHz, $CDCl_3$) δ 8.99 (d, J = 8.6 Hz, 2H), 8.67 (s, 2H), 8.43 (d, J = 8.3 Hz, 2H), 8.32 (d, J = 8.4 Hz, 2H), 8.05 (d, J = 7.2 Hz, 2H), 8.01 (d, J = 8.2 Hz, 2H), 7.29 (s, 2H), 6.60 (s, 2H), 5.31 (s, 1H), 1.82 (s, 6H). ^{13}C NMR (101 MHz, $CDCl_3$) δ 186.32, 172.15, 152.68, 149.27, 145.38, 137.05, 136.14, 134.44, 131.25, 130.55, 127.74, 127.50, 125.85, 125.36, 125.10, 118.65, 114.83, 113.50, 106.13, 101.77, 29.85, 29.82, 28.78. MS (MALDI-TOF) [m/z]: found $[M]^+$ 800.1510, calculated 800.1512 ($C_{39}H_{23}N_6O_2Ir$).

Bu-CNIr (black, yield: 30%) ^{1}H NMR (400 MHz, $CDCl_3$) δ 8.95 (2 H, d, J 8.5), 8.71 (2 H, s), 8.31 (2 H, dd, J 8.2, 0.8), 8.08 (2 H, d, J 8.6), 7.97–7.88 (2 H, m), 7.84 (2 H, s), 6.98 (2 H, dd, J 8.6, 2.0), 6.27 (2 H, d, J 1.9), 5.29 (1 H, s), 1.83 (6 H, s), 0.95 (18 H, s). ^{13}C NMR (101 MHz, $CDCl_3$) δ 185.78, 174.71, 155.37, 154.13, 146.52, 141.90, 135.66, 133.34, 131.67, 130.39, 129.09, 128.19, 124.96, 124.61, 119.21, 115.92, 112.13, 102.53, 101.46, 100.13, 34.45, 30.92, 28.90. MS (MALDI-TOF) [m/z]: found $[M]^+$ 862.2842, calculated 862.2859 ($C_{45}H_{41}N_4O_2Ir$).

DM-CNIr (black, yield: 28%) ^{1}H NMR (400 MHz, $CDCl_3$) δ 9.02 (d, J = 8.2 Hz, 2H), 8.53 (s, 2H), 8.23 (dd, J = 8.0, 1.0 Hz, 2H), 7.97 (s, 2H), 7.94–7.88 (m, 2H), 7.86 (ddd, J = 8.3, 7.1, 1.5 Hz, 2H), 6.65 (s, 2H), 4.95 (s, 1H), 2.34 (s, 6H), 1.41 (s, 6H), 1.25 (s, 6H). ^{13}C NMR (101 MHz, $CDCl_3$) δ 185.75, 173.78, 148.70, 147.08, 146.67, 135.45, 133.43, 133.07, 131.53, 130.42, 128.91, 128.28, 125.39, 124.58, 115.72, 101.25, 100.82, 29.85, 28.48, 23.97, 21.28. MS (MALDI-TOF) [m/z]: found $[M]^+$ 806.2756, calculated 806.2233 ($C_{39}H_{23}N_6O_2Ir$).